JASA ARTICLE

A modified convolution model for calculating the far field directivity of a parametric array loudspeaker

Jiaxin Zhong,[1,a] Haishan Zou,[2] Jing Lu,[2,b] and Dong Zhang[2,c]
[1]Centre for Audio, Acoustics, and Vibration, University of Technology Sydney, New South Wales 2007, Australia
[2]Key Laboratory of Modern Acoustics and Institute of Acoustics, Nanjing University, Nanjing 210093, China

ABSTRACT:
The far field directivity is a straightforward indicator to describe the radiation pattern of the audio sound generated by a parametric array loudspeaker (PAL), but its accurate and computationally efficient prediction is still challenging at present. This paper derives two-dimensional (2D), three-dimensional (3D), and 3D axisymmetric convolution models for calculating the far field directivity based on the quasilinear solution of Westervelt equation. The obtained expressions are expressed as linear and spherical convolutions of the ultrasound directivity and Westervelt directivity for 2D and 3D models, respectively. To improve prediction accuracy, the obtained expression is multiplied by an effective directivity resulted from the aperture factor of audio sound. The calculated directivities are compared against the exact solution obtained using the cylindrical and spherical wave expansions for 2D and 3D models, respectively. Numerical results with piston, apodized, and steerable profiles in both 2D and 3D models show that the proposed modified convolution model agrees well with the exact solution. It is also found that sidelobes appear in the audio sound directivity at large aperture sizes and high audio frequencies due to the aperture factor of audio sound, which can be predicted with the proposed method with a relatively low computational expenditure.
 https://doi.org/10.1121/10.0017361
(Received 17 October 2022; revised 25 January 2023; accepted 7 February 2023; published online 1 March 2023)
[Editor: Mark F. Hamilton] Pages: 1439–1451

I. INTRODUCTION

Parametric array loudspeakers (PALs) are an application of the parametric acoustic array in air and known for their exceptional directionality at low frequencies.[1,2] They have been used in many audio applications including active noise control,[3,4] sound reproduction,[5] sound absorption measurement,[6] and so on. In recent years, there is a growing interest in the development of a steerable PAL which aims to steer the highly directional audio beam in a desired direction without the need to mechanically rotate the source.[7–10] The far field directivity of the audio sound generated by a PAL is an important indicator to describe the radiation pattern of the PAL, but it is still challenging to be accurately predicted with a low computational expenditure, which will be addressed in this paper.

The audio sound field generated by a PAL is more complicated when compared to a conventional dynamic loudspeaker because the parametrical generation is nonlinear in nature. The audio sound field on the front side was proposed to be divided into three regions: the near field, the Westervelt far field, and the inverse-law far field.[11] In the near field, the local nonlinearity caused by ultrasound is strong resulting in fluctuations in the audio sound pressure. The general second-order nonlinear wave equation is required to model the wave propagation in the near field.[12,13] Its equivalent form expressed in terms of the velocity potential (Kuznetsov equation) is more often used because the difficult evaluation of the spatial derivatives of the ultrasonic Lagrangian density can be avoided.[11,13] Alternatively, an algebraic correction for the quasilinear solution of Westervelt equation was proposed to include the local nonlinearity requiring less computational cost.[14] In the Westervelt far field, Westervelt equation is sufficiently accurate to describe the wave propagation, and various kinds of numerical methods have been proposed in the literature.[15,16] It is noted that many contributions have been made to enable a fast calculation of the audio sound in the paraxial region in the Westervelt far field at the cost of prediction accuracies.[17,18]

This work focuses on numerical models in the inverse-law far field, where the audio sound pressure is inversely proportional to the propagation distance. The audio sound directivity in the inverse-law far field is a straightforward indicator to characterize the radiation pattern of a PAL. Although the methods for calculating the audio sound in the near field and the Westervelt far field are also exploitable to calculate the far field directivity, the calculation is rather complicated and time-consuming. A simple closed-form expression for directivity was first obtained by Westervelt in 1963, and is now termed Westervelt directivity.[19] The expression shows that the directivity is determined by the audio frequency and the ultrasonic attenuation coefficient due to atmospheric absorption. The accuracy of Westervelt directivity was then improved by Berktay and Leahy by taking into account the aperture factor and the wave shape.[20,21] However, they are only applicable for a piston source which

[a]Present address: Graduate Program in Acoustics, College of Engineering, The Pennsylvania State University, University Park, PA 16802, USA.
[b]Also at: NJU-Horizon Intelligent Audio Laboratory, Horizon Robotics, Nanjing 210038, China.
[c]Electronic mail: dzhang@nju.edu.cn

means the velocity profile is uniform on the radiation surface. In 2006, a product directivity model was used by Gan *et al.* to estimate the radiation pattern of a steerable PAL, which approximates the audio sound directivity by the product of the directivity of two ultrasonic waves.[22] This model provides the basis for calculating the far field directivity of a PAL other than a piston source, such as a steerable PAL. The sidelobe level predicted by the product directivity model was found to be much smaller than measurements because the diffraction of audio sound waves was neglected in the model, which was then addressed to some extent by using an equivalent Gaussian source array.[23] A transformed Khokhlov–Zabolotskaya–Kuznetsov (KZK) equation was also used to calculate the far field by using a finite difference method, but the obtained results are accurate only within a small angle due to the paraxial assumption.[24]

To date, the most accurate and computationally efficient numerical model for calculating the far field directivity was proposed by Shi and Kajikawa in 2015.[25] The fundamental idea is that a PAL emits infinitely many ultrasonic beams in air, and the audio sound generated in each direction has a beam pattern of Westervelt directivity weighted by the amplitude of ultrasonic waves in this direction. Accordingly, the total audio directivity is the summation of all contributed audio beam patterns resulting in a convolution of Westervelt directivity and ultrasonic directivities, so it is now termed the convolution model. It was reported to provide better agreement with measurement and proved to be a powerful tool for the directivity control of a steerable PAL[7] and the prediction of the harmonic distortion of modulation algorithms.[26] However, the convolution model proposed in Ref. 25 is valid only for a two-dimensional (2D) radiation problem, so it was used only for the applications of a linear phased array PAL. In addition, the phase of Westervelt directivity is neglected, which may result in inaccurate predictions as discussed in Ref. 27. The three-dimensional (3D) convolution model was also derived in Ref. 27, but the convolution in the azimuthal direction is not taken into account. In the convolution model, the complicated ultrasound pressure in the near field is simply approximated by its inward-extrapolated far field pressure. This approximation is only accurate in the far field of the ultrasound field which is considered to be beyond the Rayleigh distance.[28] Accordingly, the nonlinear interactions of ultrasonic waves in the near field cannot be correctly described resulting in an inaccurate prediction of the audio sound directivity. The inaccuracy is more significant at larger aperture sizes and/or higher ultrasound frequencies because of a larger Rayleigh distance.

This work derives 2D, 3D, and 3D axisymmetric convolution models for calculating the far field directivity based on the quasilinear solution of Westervelt equation. To improve the prediction accuracy of the directivity, the obtained expression is multiplied by an effective directivity resulted from the aperture factor of audio sound. Numerical results with piston, apodized, and steerable profiles in both 2D and 3D models are presented and compared to the exact solution to verify the proposed methods.

II. QUASILINEAR SOLUTION BASED ON WESTERVELT EQUATION

Figure 1 shows the sketch of a 2D and 3D baffled steerable PAL radiating ultrasound in free space. In the 2D model, rectangular (x, y) and polar (ρ, φ) coordinate systems are established with their origin, O, at the centroid of the PAL, and the positive x axis pointing to the radiation direction, where ρ and φ are the radial and azimuthal coordinates, respectively. The 2D model is identical to the 3D model when one dimension of the PAL is much larger than the wavelength.[16] It was usually used for modeling the radiation from a linear phased array PAL.[25] The half width of the PAL along the y axis is denoted by a. The velocity profile for the ultrasound on the source line $x = 0$ is

$$v(\boldsymbol{\rho}_s) = v_0 u_1(\boldsymbol{\rho}_s) e^{-i\omega_1 t} + v_0 u_2(\boldsymbol{\rho}_s) e^{-i\omega_2 t}, \quad \rho_s \le a, \tag{1}$$

where i is the imaginary unit, v_0 is a constant with a unit of m/s, $u_i(\boldsymbol{\rho}_s)$ is an arbitrary complex velocity profile at the source point $\boldsymbol{\rho}_s = (x_s, y_s)$ with $y_s = 0$, $\omega_i = 2\pi f_i$ is the angular ultrasound frequency, f_i is the ultrasound frequency with $f_2 > f_1$, the subscript i represents the ultrasound index, $i = 1, 2$, and t is the time.

In the 3D model, Cartesian (x, y, z) and spherical (r, θ, φ) coordinate systems are established with their origin, O, at the centroid of the PAL, and the positive z axis pointing

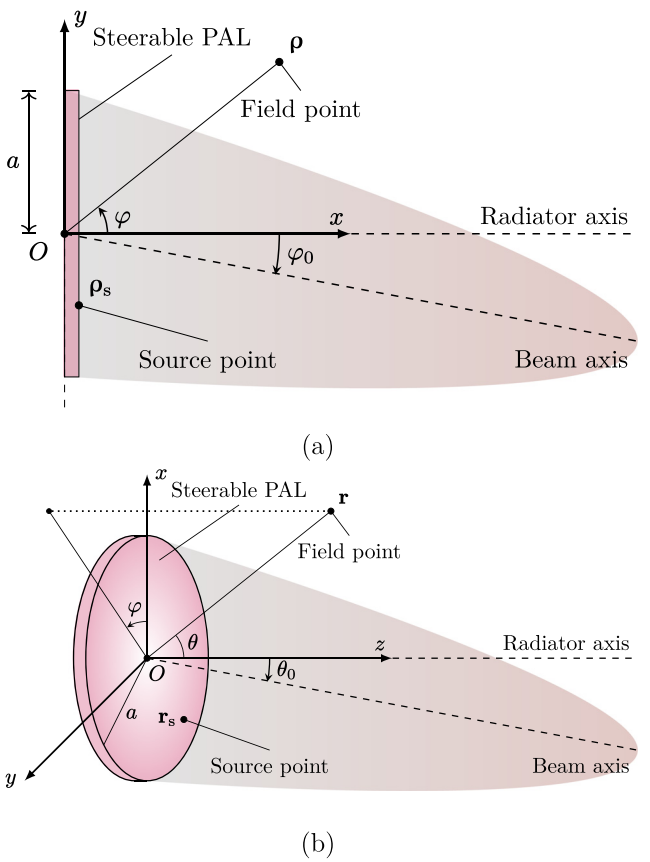

FIG. 1. (Color online) Sketch of steerable PALs. (a) 2D model, (b) 3D model.

https://doi.org/10.1121/10.0017361

to the radiation direction, where r, θ, and φ, are the radial, zenithal, and azimuthal coordinates, respectively. In this work, a circular PAL with a radius a is considered because it can be efficiently solved using the spherical wave expansion method as described in Sec. II B.[15] It is noted that the proposed model is also applicable for the PAL with other shapes, such as the rectangular PAL. The boundary condition for the ultrasound on the source plane $z = 0$ is

$$v(\mathbf{r}_s) = v_0 u_1(\mathbf{r}_s)\mathrm{e}^{-\mathrm{i}\omega_1 t} + v_0 u_2(\mathbf{r}_s)\mathrm{e}^{-\mathrm{i}\omega_2 t}, \quad r_s \le a, \tag{2}$$

where $u_i(\mathbf{r}_s)$ is an arbitrary complex velocity profile at the source point $\mathbf{r}_s = (x_s, y_s, z_s)$ for the ultrasound at the frequency f_i with $z_s = 0$. In the 3D axisymmetric model, the velocity profile is axisymmetric, such as the radiation from a circular piston source.

A. Two-dimensional (2D) model

The accurate modeling of the PAL subject to the second-order nonlinearity in the far field is governed by Westervelt equation. By using the successive method, the quasilinear solution of the audio sound is modeled as the radiation from an infinitely large virtual source with the source density being[16]

$$q_a(\boldsymbol{\rho}_v) = \frac{\beta k_a}{\mathrm{i}\rho_0^2 c_0^3} p_1^*(\boldsymbol{\rho}_v) p_2(\boldsymbol{\rho}_v), \tag{3}$$

at the virtual source point $\boldsymbol{\rho}_v = (x_v, y_v)$, where the superscript * represents the complex conjugate, ρ_0 is the air density, c_0 is the linear sound speed in air, β is the nonlinearity coefficient, $k_a = \omega_a/c_0$ is the audio wavenumber, $\omega_a = 2\pi f_a$ is the audio angular frequency, and $f_a = f_2 - f_1$ is the audio frequency. The ultrasound pressure at the virtual source point is obtained using a Rayleigh-like integral[16]

$$p_i(\boldsymbol{\rho}_v) = \frac{p_0}{2}\int_{-a}^{a} H_0(k_i|\boldsymbol{\rho}_v - \boldsymbol{\rho}_s|) u_i(\boldsymbol{\rho}_s) k_i \mathrm{d}y_s, \tag{4}$$

where $p_0 = \rho_0 c_0 v_0$ is the on-surface pressure amplitude, $k_i = \omega_i/c_0 + \mathrm{i}\alpha_i$ is the complex wavenumber of the ultrasound at the frequency of f_i, α_i is the ultrasound attenuation coefficient due to atmospheric absorption, and $H_0(\cdot)$ is the Hankel function of order 0.

The audio sound pressure at a field point $\boldsymbol{\rho} = (x, y)$ is then obtained as[16]

$$p_a(\boldsymbol{\rho}) = \frac{\rho_0 c_0 k_a}{4}\int_0^{2\pi}\int_0^{\infty} q_a(\boldsymbol{\rho}_v) H_0(k_a|\boldsymbol{\rho} - \boldsymbol{\rho}_v|)\rho_v \mathrm{d}\rho_v \mathrm{d}\varphi_v. \tag{5}$$

Equation (5) is hard to evaluate the far field directivity because of the numerical integration of highly oscillatory integrands. By using the cylindrical wave expansion,[16] the directivity can be obtained as

$$\mathcal{D}_a(\varphi) = \sum_{m_a=-\infty}^{\infty} A_{m_a}\mathrm{e}^{\mathrm{i}m_a\varphi}, \tag{6}$$

where the coefficients are

$$A_{m_a} = \mathrm{i}^{-m_a}\sum_{m_1=-\infty}^{\infty}\int_0^{\infty}\mathcal{R}_{m_1}^*(\rho_v)\mathcal{R}_{m_2}(\rho_v)J_{m_a}(k_a\rho_v)k_a^2\rho_v \mathrm{d}\rho_v. \tag{7}$$

In Eq. (7), $J_{m_a}(\cdot)$ represents the Bessel function of order m_a, $m_2 = m_1 + m_a$, and the radial component for ultrasound is

$$\mathcal{R}_{m_i}(\rho) = \int_0^a \bar{u}_{m_i}(\rho_s) J_{m_i}(k_i\rho_{s,<}) H_{m_i}(k_i\rho_{s,>}) k_i \mathrm{d}\rho_s, \tag{8}$$

where $\rho_{s,<} = \min(\rho, \rho_s)$, $\rho_{s,>} = \max(\rho, \rho_s)$, the effective velocity profile is

$$\bar{u}_{m_i}(\rho_s) = \frac{1}{2}[\mathrm{i}^{-m_i}u_i(0, \rho_s) + \mathrm{i}^{m_i}u_i(0, -\rho_s)]. \tag{9}$$

It is noted that the cylindrical expansion of the audio sound directivity given by Eq. (6) is equivalent to the exact solution of Eq. (5) but with a relatively low computational expenditure. It will be used to calculate the exact solution of the far field directivity in a 2D model.

B. Three-dimensional (3D) model

In the 3D model, the source density at a virtual source point $\mathbf{r}_v = (x_v, y_v, z_v)$ is similar to Eq. (3) and expressed as[15]

$$q_a(\mathbf{r}_v) = \frac{\beta k_a}{\mathrm{i}\rho_0^2 c_0^3} p_1^*(\mathbf{r}_v) p_2(\mathbf{r}_v). \tag{10}$$

The ultrasound pressure at a virtual source point $\mathbf{r}_v$ is calculated by Rayleigh integral as[15]

$$p_i(\mathbf{r}_v) = \frac{p_0 k_i}{2\pi\mathrm{i}}\int_0^{2\pi}\int_0^a u_i(\mathbf{r}_s)\frac{\mathrm{e}^{\mathrm{i}k_i|\mathbf{r}_v - \mathbf{r}_s|}}{|\mathbf{r}_v - \mathbf{r}_s|} r_s \mathrm{d}r_s \mathrm{d}\varphi_s. \tag{11}$$

The audio sound pressure at a field point $\mathbf{r} = (x, y, z)$ is then obtained as[15]

$$p_a(\mathbf{r}) = \frac{\rho_0 c_0 k_a}{4\mathrm{i}\pi}\int_0^{2\pi}\int_0^{\pi}\int_0^{\infty} q_a(\mathbf{r}_v)\frac{\mathrm{e}^{\mathrm{i}k_a|\mathbf{r} - \mathbf{r}_v|}}{|\mathbf{r} - \mathbf{r}_v|} r_v^2 \sin\theta_v \mathrm{d}r_v \mathrm{d}\theta_v \mathrm{d}\varphi_v. \tag{12}$$

The direct calculation of the audio sound pressure involves the numerical evaluation of a fivefold integral after substituting Eqs. (10) and (11) into Eq. (12), which is rather time-consuming. The spherical wave expansion (SWE) was proposed to efficiently calculate the audio sound pressure without loss of accuracy, so it is summarized here.[15,29] For an arbitrary velocity profile $u_i(\mathbf{r}_s)$, the use of the SWE requires a decomposition of the profile into Zernike circular polynomials[29]

$$u_i(\mathbf{r}_s) = \sum_{n_i=0}^{\infty}\sum_{m_i=-n_i}^{n_i}{}' M_{n_i}^{m_i} R_{n_i}^{m_i}(r_s/a)\mathrm{e}^{\mathrm{i}m_i\varphi_s}, \tag{13}$$

where the prime over the summation sign indicates that the summation is over only when $n_i - m_i$ is even, $R_{n_i}^{m_i}(r_s/a)$ is the Zernike radial polynomial of degree n_i and azimuthal

order m_i, and the coefficients $M_{n_i}^{m_i}$ are Zernike moments. For an axisymmetric profile, $M_{n_i}^{m_i} \neq 0$ only when $n_i = m_i = 0$. The audio sound directivity can be obtained as[29]

$$\mathcal{D}_{\mathrm{a}}(\theta,\varphi) = \sum_{n_1,n_2=0}^{\infty} \sum_{m_1=-n_1}^{n_1\prime} \sum_{m_2=-n_2}^{n_2\prime} M_{n_1}^{m_1,*} M_{n_2}^{m_2} \sum_{\ell_{\mathrm{a}}=0}^{\infty} A_{\ell_{\mathrm{a}}}^{n,m} Y_{2\ell_{\mathrm{a}}+|m_{\mathrm{a}}|}^{m_{\mathrm{a}}}(\theta,\varphi), \tag{14}$$

where $m_{\mathrm{a}} = m_2 - m_1$, $Y_{2\ell_{\mathrm{a}}+|m_{\mathrm{a}}|}^{m_{\mathrm{a}}}(\theta,\varphi)$ are spherical harmonics, and the coefficient is

$$\begin{aligned} A_{\ell_{\mathrm{a}}}^{n,m} = & \sum_{\ell_1,\ell_2=0}^{\infty} (-1)^{m_2+\ell_{\mathrm{a}}} \mathrm{i}^{-|m_{\mathrm{a}}|-1} Y_{2\ell_1+|m_1|}^{m_1}(\pi/2,0) Y_{2\ell_2+|m_2|}^{m_2}(\pi/2,0) \\ & \times \sqrt{\frac{(4\ell_1+2|m_1|+1)(4\ell_2+2|m_2|+1)(4\ell_{\mathrm{a}}+2|m_{\mathrm{a}}|+1)}{4\pi}} \\ & \times \begin{pmatrix} 2\ell_1+|m_1| & 2\ell_2+|m_2| & 2\ell_{\mathrm{a}}+|m_{\mathrm{a}}| \\ 0 & 0 & 0 \end{pmatrix} \begin{pmatrix} 2\ell_1+|m_1| & 2\ell_2+|m_2| & 2\ell_{\mathrm{a}}+|m_{\mathrm{a}}| \\ -m_1 & m_2 & -m_{\mathrm{a}} \end{pmatrix} \\ & \times \int_0^{\infty} \mathcal{R}_{2\ell_1+|m_1|}^{n_1,m_1,*}(r_{\mathrm{v}}) \mathcal{R}_{2\ell_2+|m_2|}^{n_2,m_2}(r_{\mathrm{v}}) \mathrm{j}_{2\ell_{\mathrm{a}}+|m_{\mathrm{a}}|}(k_{\mathrm{a}} r_{\mathrm{v}}) k_{\mathrm{a}}^3 r_{\mathrm{v}}^2 \mathrm{d}r_{\mathrm{v}}. \end{aligned} \tag{15}$$

In Eq. (15), $\begin{pmatrix} j_1 & j_2 & j_3 \\ \mu_1 & \mu_2 & \mu_3 \end{pmatrix}$ is the Wigner 3j symbol, and the radial component for ultrasound is

$$\mathcal{R}_{2\ell_i+|m_i|}^{n_i,m_i} = \int_0^a R_{n_i}^{m_i}(r_{\mathrm{s}}/a) \mathrm{j}_{2\ell_i+|m_i|}(k_i r_{\mathrm{s},<}) \mathrm{h}_{2\ell_i+|m_i|}(k_i r_{\mathrm{s},>}) k_i^2 r_{\mathrm{s}} \mathrm{d}r_{\mathrm{s}}, \tag{16}$$

where $r_{\mathrm{s},<} = \min(r, r_{\mathrm{s}})$, $r_{\mathrm{s},>} = \max(r, r_{\mathrm{s}})$, $\mathrm{j}_\ell(\cdot)$ and $\mathrm{h}_\ell(\cdot)$ are spherical Bessel and Hankel functions of order ℓ, respectively, The SWE will be used to calculate the exact solution of the far field directivity in 3D and 3D axisymmetric models.

III. CONVOLUTION MODEL

A. 2D model

The ultrasound pressure given by Eq. (4) in the far field, $\rho_{\mathrm{v}} \to \infty$, can be written as[30]

$$p_i(\boldsymbol{\rho}_{\mathrm{v}}) = \sqrt{\frac{2}{\mathrm{i}\pi k_i \rho_{\mathrm{v}}}} p_0 k_i a \mathrm{e}^{\mathrm{i}k_i\rho_{\mathrm{v}}} \mathcal{D}_i(\varphi_{\mathrm{v}}), \tag{17}$$

where the amplitude is chosen to ensure the ultrasound directivity $\mathcal{D}_i(\varphi_{\mathrm{v}}) = 1$ at the mainlobe. The key of convolution models is to approximate the exact ultrasound field Eq. (4) by the inward-extrapolated far field pressure given by Eq. (17). The source density of audio sound is then obtained by substituting Eq. (17) into Eq. (3) yielding

$$q_{\mathrm{a}}(\boldsymbol{\rho}_{\mathrm{v}}) = \frac{2\beta p_0^2 k_{\mathrm{a}} \sqrt{k_1 k_2} a^2}{\mathrm{i}\pi \rho_0^2 c_0^3 \rho_{\mathrm{v}}} \mathrm{e}^{\mathrm{i}(k_2 - k_1^*)\rho_{\mathrm{v}}} \mathcal{D}_1^*(\varphi_{\mathrm{v}}) \mathcal{D}_2(\varphi_{\mathrm{v}}). \tag{18}$$

The substitution of Eq. (18) into Eq. (5) yields

$$p_{\mathrm{a}}(\boldsymbol{\rho}) = \frac{\beta p_0^2 k_{\mathrm{a}}^2 \sqrt{k_1 k_2} a^2}{2\pi \mathrm{i} \rho_0 c_0^2} \int_0^{2\pi} \int_0^{\infty} \mathcal{D}_1^*(\varphi_{\mathrm{v}}) \mathcal{D}_2(\varphi_{\mathrm{v}}) \times \mathrm{e}^{\mathrm{i}(k_2 - k_1^*)\rho_{\mathrm{v}}} H_0(k_{\mathrm{a}}|\boldsymbol{\rho} - \boldsymbol{\rho}_{\mathrm{v}}|) \rho_{\mathrm{v}} \mathrm{d}\rho_{\mathrm{v}} \mathrm{d}\varphi_{\mathrm{v}}. \tag{19}$$

In the far field, $\rho \to \infty$, the Hankel function in Eq. (19) can be approximated by its limiting form as

$$\begin{aligned} H_0(k_{\mathrm{a}}|\boldsymbol{\rho} - \boldsymbol{\rho}_{\mathrm{v}}|) &\approx \sqrt{\frac{2}{\mathrm{i}\pi k_{\mathrm{a}}}} \frac{\mathrm{e}^{\mathrm{i}k_{\mathrm{a}}|\boldsymbol{\rho}-\boldsymbol{\rho}_{\mathrm{v}}|}}{\sqrt{|\boldsymbol{\rho} - \boldsymbol{\rho}_{\mathrm{v}}|}} \\ &\approx \sqrt{\frac{2}{\mathrm{i}\pi k_{\mathrm{a}} \rho}} \mathrm{e}^{\mathrm{i}k_{\mathrm{a}}[\rho - \rho_{\mathrm{v}} \cos(\varphi - \varphi_{\mathrm{v}})]}, \end{aligned} \tag{20}$$

where the following approximation has been used:

$$|\boldsymbol{\rho} - \boldsymbol{\rho}_{\mathrm{v}}| \approx \rho - \frac{\boldsymbol{\rho} \cdot \boldsymbol{\rho}_{\mathrm{v}}}{\rho} = \rho - \rho_{\mathrm{v}} \cos(\varphi - \varphi_{\mathrm{v}}). \tag{21}$$

The substitution of Eq. (20) into Eq. (19) yields

$$p_{\mathrm{a}}(\boldsymbol{\rho}) = \frac{\beta p_0^2 k_{\mathrm{a}}^2 a^2}{\mathrm{i}\pi} \sqrt{\frac{k_1 k_2}{2\pi \mathrm{i} k_{\mathrm{a}} \rho}} \mathrm{e}^{\mathrm{i}k_{\mathrm{a}}\rho} \int_0^{2\pi} \int_0^{\infty} \mathcal{D}_1^*(\varphi_{\mathrm{v}}) \mathcal{D}_2(\varphi_{\mathrm{v}}) \times \mathrm{e}^{\mathrm{i}\left[k_2 - k_1^* - k_{\mathrm{a}} \cos(\varphi - \varphi_{\mathrm{v}})\right]\rho_{\mathrm{v}}} \mathrm{d}\rho_{\mathrm{v}} \mathrm{d}\varphi_{\mathrm{v}}. \tag{22}$$

We define an integral which is termed Westervelt directivity as

$$\begin{aligned} \mathcal{D}_{\mathrm{W}}(\gamma) &\equiv \alpha_{\mathrm{t}} \int_0^{\infty} \mathrm{e}^{\mathrm{i}(k_2 - k_1^* - k_{\mathrm{a}} \cos\gamma)\rho_{\mathrm{v}}} \mathrm{d}\rho_{\mathrm{v}} \\ &= \frac{1}{1 - \mathrm{i}k_{\mathrm{a}} \alpha_{\mathrm{u}}^{-1} \sin^2(\gamma/2)}, \end{aligned} \tag{23}$$

where the total attenuation coefficient $\alpha_{\mathrm{t}} \equiv \alpha_1 + \alpha_2$ is multiplied to normalize $\mathcal{D}_{\mathrm{W}}(\gamma)$ at $\gamma = 0$, i.e., $\mathcal{D}_{\mathrm{W}}(0) = 1$, and the

https://doi.org/10.1121/10.0017361

averaged attenuation coefficient is defined as $\alpha_u \equiv \alpha_t/2$. Equation (22) then reduces to

$$p_a(\boldsymbol{\rho}) = \frac{\beta p_0^2 k_a^2 a^2}{\pi i \alpha_t}\sqrt{\frac{k_1 k_2}{2\pi i k_a \rho}} e^{ik_a\rho}\mathcal{D}_a(\varphi), \tag{24}$$

where the audio sound directivity is written as

$$\begin{aligned}\mathcal{D}_a(\varphi) &= (\mathcal{D}_1^*\mathcal{D}_2 * \mathcal{D}_W)(\varphi)\\ &= \int_0^{2\pi} \mathcal{D}_1^*(\varphi_v)\mathcal{D}_2(\varphi_v)\mathcal{D}_W(\varphi-\varphi_v)d\varphi_v.\end{aligned} \tag{25}$$

In Eq. (25), "*" denotes the linear convolution operator. Equation (25) is termed the direct convolution model which shows that the audio sound directivity is the convolution of Westervelt directivity and the product directivity of ultrasound. A similar form has been proposed in Ref. 25 in a geometric way. The phase of Westervelt directivity is neglected in Ref. 25 which may result in inaccurate predictions as discussed in Ref. 27. Compared to Ref. 25, the convolution model given by Eq. (25) in this work is derived in a more rigorous way based on the quasilinear solution of Westervelt equation. A key step in the direct convolution model is that the ultrasound field is approximated by its inward-extrapolated far field pressure as shown by Eq. (17). This approximation is only accurate in the far field which is considered to be beyond Rayleigh distance.[28] Accordingly, the nonlinear interactions of ultrasonic waves in the near field cannot be correctly captured resulting in an inaccurate prediction of far field directivity of audio sound. The accuracy of the audio sound directivity obtained using the direct convolution model given by Eq. (25) can be improved by taking into account the aperture factor of audio sound, and the directivity is modified as

$$\tilde{\mathcal{D}}_a(\varphi) = \mathcal{D}_A(\varphi)\mathcal{D}_a(\varphi) = \mathcal{D}_A(\varphi)(\mathcal{D}_1^*\mathcal{D}_2 * \mathcal{D}_W)(\varphi), \tag{26}$$

where the effective directivity $\mathcal{D}_A(\varphi)$ is the far field directivity of an audio source with a same aperture size and a velocity profile of $u_a(\boldsymbol{\rho}_s) = u_1^*(\boldsymbol{\rho}_s)u_2(\boldsymbol{\rho}_s)$. The audio sound directivity obtained using Eq. (26) is termed the modified convolution model in this work.

B. 3D model

In the 3D model as shown in Fig. 1(b), the ultrasound pressure given by Eq. (11) in the far field, $r_v \to \infty$, is written as[30]

$$p_i(\mathbf{r}_v) = \frac{p_0 k_i a^2}{2ir_v} e^{ik_i r_v}\mathcal{D}_i(\theta_v, \varphi_v), \tag{27}$$

where the amplitude is chosen to ensure the ultrasound directivity $\mathcal{D}_i(\theta, \varphi) = 1$ at the mainlobe. The source density of audio sound is then obtained by substituting Eq. (27) into Eq. (10) yielding

$$q_a(\mathbf{r}_v) = \frac{\beta p_0^2 k_1 k_2 k_a a^4}{4i\rho_0^2 c_0^3 r_v^2}\mathcal{D}_1^*(\theta_v, \varphi_v)\mathcal{D}_2(\theta_v, \varphi_v)e^{i(k_2-k_1^*)r_v}. \tag{28}$$

The substitution of Eq. (28) into Eq. (12) yields

$$\begin{aligned}p_a(\mathbf{r}) = -\frac{\beta p_0^2 k_1 k_2 k_a^2 a^4}{16\pi\rho_0 c_0^2}\int_0^{2\pi}\int_0^{\pi}\int_0^{\infty}\mathcal{D}_1^*(\theta_v, \varphi_v)\mathcal{D}_2(\theta_v, \varphi_v)\\ \times e^{i(k_2-k_1^*)r_v}\frac{e^{ik_a|\mathbf{r}-\mathbf{r}_v|}}{|\mathbf{r}-\mathbf{r}_v|}\sin\theta_v dr_v d\theta_v d\varphi_v.\end{aligned} \tag{29}$$

In the far field, $r \to \infty$, the Green's function in Eq. (29) can be approximated by its limiting form as

$$\frac{e^{ik_a|\mathbf{r}-\mathbf{r}_v|}}{|\mathbf{r}-\mathbf{r}_v|} \approx \frac{1}{r}e^{ik_a(r-r_v\cos\gamma)}, \tag{30}$$

where the following approximation has been used:

$$|\mathbf{r}-\mathbf{r}_v| \approx r - \frac{\mathbf{r}\cdot\mathbf{r}_v}{r} = r - r_v\cos\gamma, \tag{31}$$

with the angle between vectors $\mathbf{r}$ and $\mathbf{r}_v$ as

$$\cos\gamma = \cos\theta\cos\theta_v + \sin\theta\sin\theta_v\cos(\varphi-\varphi_v). \tag{32}$$

The substitution of Eq. (30) into Eq. (29) with the definition of Westervelt directivity given by Eq. (23) yields

$$p_a(\mathbf{r}) = -\frac{\beta p_0^2 k_1 k_2 k_a^2 a^4}{16\pi\alpha_t r}e^{ik_a r}\mathcal{D}_a(\theta, \varphi), \tag{33}$$

where the audio sound directivity is written as

$$\begin{aligned}\mathcal{D}_a(\theta, \varphi) &= (\mathcal{D}_1^*\mathcal{D}_2 \circledast \mathcal{D}_W)(\theta, \varphi)\\ &= \int_0^{2\pi}\int_0^{\pi}\mathcal{D}_1^*(\theta_v, \varphi_v)\mathcal{D}_2(\theta_v, \varphi_v)\\ &\quad\times \mathcal{D}_W(\gamma)\sin\theta_v d\theta_v d\varphi_v.\end{aligned} \tag{34}$$

It is noted that the functions $\mathcal{D}_1^*(\theta, \varphi)\mathcal{D}_2(\theta, \varphi)$ and $\mathcal{D}_W(\gamma)$ are defined on a unit sphere with the zenithal and azimuthal angles of θ and φ, respectively. Therefore, the audio sound directivity can be seen as a spherical convolution[31] between them as shown by Eq. (34), where "$\circledast$" denotes the spherical convolution operator. Similar to Eq. (26), the 3D modified convolution model is obtained by taking into account the aperture factor of audio sound as

$$\tilde{\mathcal{D}}_a(\theta, \varphi) = \mathcal{D}_A(\theta, \varphi)(\mathcal{D}_1^*\mathcal{D}_2 \circledast \mathcal{D}_W)(\theta, \varphi), \tag{35}$$

where the effective directivity $\mathcal{D}_A(\theta, \varphi)$ is the far field directivity of an audio source with a same aperture size and a velocity profile of $u_a(\mathbf{r}_s) = u_1^*(\mathbf{r}_s)u_2(\mathbf{r}_s)$.

The geometric interpretation of the direct convolution model given by Eq. (34) is that the PAL emits infinitely many ultrasonic waves in all directions and the audio sound directivity in each direction (θ_v, φ_v) has a form of Westervelt directivity weighted by ultrasonic directivity $\mathcal{D}_1^*(\theta_v, \varphi_v)\mathcal{D}_2(\theta_v, \varphi_v)$. The argument of Westervelt directivity γ is the included angle

between the direction of field and virtual source points, i.e., (θ, φ) and (θ_v, φ_v). A similar form of Eq. (34) has been derived in Ref. 27 in a geometric way, where γ is chosen as the included angle between the zenithal angles θ and θ_v. This leads to inaccurate predictions because the convolution in the azimuthal direction is not included.

C. 3D axisymmetric model

In the 3D axisymmetric model, the velocity profile of ultrasound $u_i(\mathbf{r}_s)$ is independent of the azimuthal angle φ_s. Consequently, the audio sound directivity is axisymmetric and is independent of φ. By setting $\varphi = 0$ in Eq. (32) and using Westervelt directivity given by Eq. (23), the integration with respect to the azimuthal angle φ_v can be simplified to (see Appendix for derivations)

$$\frac{1}{2\pi}\int_0^{2\pi} \frac{\mathrm{d}\varphi_v}{1 - \mathrm{i}k_a\alpha_t^{-1}(1 - \cos\theta\cos\theta_v - \sin\theta\sin\theta_v\cos\varphi_v)} = \sqrt{\mathcal{D}_W(\theta - \theta_v)}\sqrt{\mathcal{D}_W(\theta + \theta_v)}. \quad (36)$$

The 3D axisymmetric direct convolution model is then obtained by substituting Eq. (36) into Eq. (34) as

$$\mathcal{D}_a(\theta) = \int_0^{\pi} \mathcal{D}_1^*(\theta_v)\mathcal{D}_2(\theta_v)\sqrt{\mathcal{D}_W(\theta - \theta_v)} \times \sqrt{\mathcal{D}_W(\theta + \theta_v)}\sin\theta_v \mathrm{d}\theta_v, \quad (37)$$

which cannot be written using the convolution operator. The 3D axisymmetric modified convolution model is then

$$\tilde{\mathcal{D}}_a(\theta) = \mathcal{D}_A(\theta)\int_0^{\pi} \mathcal{D}_1^*(\theta_v)\mathcal{D}_2(\theta_v)\sqrt{\mathcal{D}_W(\theta - \theta_v)} \times \sqrt{\mathcal{D}_W(\theta + \theta_v)}\sin\theta_v \mathrm{d}\theta_v, \quad (38)$$

where the effective directivity $\mathcal{D}_A(\theta)$ is the far field directivity of an axisymmetric audio source with a same aperture size and an axisymmetric velocity profile.

The geometric interpretation of Eq. (37) is that the PAL emits infinitely many ultrasonic waves in all directions and the audio sound directivity in each zenithal direction θ_v has a form of $\sqrt{\mathcal{D}_W(\theta - \theta_v)}\sqrt{\mathcal{D}_W(\theta + \theta_v)}$ weighted by ultrasonic directivity $\mathcal{D}_1^*(\theta_v)\mathcal{D}_2(\theta_v)$. According to Eq. (36), it is seen that $\sqrt{\mathcal{D}_W(\theta - \theta_v)}\sqrt{\mathcal{D}_W(\theta + \theta_v)}$ represents an effective Westervelt directivity generated by a highly collimated spherical cone source on the surface $\theta = \theta_v$. A 3D axisymmetric direct convolution model was also given in Ref. 27 similar to Eq. (37) in this work, but Westervelt directivity given by Eq. (23) is used which represents the directivity generated by a highly collimated line source.

IV. NUMERICAL EXAMPLES

Numerical simulations are conducted using MATLAB (MathWorks, Natick, MA) R2022a in this work. The sound attenuation coefficient due to atmospheric absorption is calculated according to ISO 9613-1, with a relative humidity of 70% and temperature 20° C.[32] The average ultrasound frequency $f_u = (f_1 + f_2)/2$ is set to 40 kHz. For better comparison, the directivity obtained using the cylindrical and spherical wave expansions given by Eqs. (6) and (14), respectively, is denoted as "Exact solution" in this work. The directivity obtained using the direct convolution model given by Eqs. (25), (34), and (37) is denoted as "Direct convolution model." The directivity obtained using the modified convolution model given by Eqs. (26), (35), and (38) is denoted as "Modified convolution model." The obtained directivities are normalized at the mainlobe and presented in decibels.

A. 2D model

1. Piston source

For a piston source in a 2D model, the velocity profile is uniform for ultrasound $u_i(\boldsymbol{\rho}_s) = 1$, where $\rho_s \le a$. Accordingly, the far field directivity of ultrasound is $\mathcal{D}_i(\varphi) = \mathrm{sinc}(k_i a \sin\varphi)$, where $\mathrm{sinc}(x) \equiv (\sin x)/x$ is the sinc function. The aperture factor of audio sound is determined by an audio source with a same aperture size and a velocity profile of $u_a(\boldsymbol{\rho}_s) = 1$. The effective directivity is then $\mathcal{D}_A(\varphi) = \mathrm{sinc}(k_a a \sin\varphi)$. Figure 2 shows the audio sound directivities generated by such a PAL obtained using different methods, where Westervelt directivity is also presented for comparison. It is observed that the directivity obtained using different methods is accurate in the vicinity of the mainlobe, but shows inaccuracies at large azimuthal angles. The directivity obtained using the modified convolution model agrees better with the exact solution. For simplicity, an indicator of 0.1 dB (or 1 dB) error beam width is defined as the angular separation in which the error of the calculated directivity is 0.1 dB (or 1 dB) from the mainlobe. At 400 Hz, as shown in the top row of Fig. 2, the error of the modified convolution model is less than 0.1 dB at all angles, so the 0.1 dB error beam width is 180°. However, it reduces to only 93°, 43°, and 60° for the direct convolution model when the aperture size is 5, 10, and 20 cm, respectively. The improvement of the modified convolution model is also presented at high audio frequencies. At 4 kHz, as shown in the bottom row of Fig. 2, the 1 dB error beam width for the modified convolution model is 78°, 41°, and 23°, when the aperture size is 5, 10, and 20 cm, respectively, but it decreases to 28°, 14°, and 7° for the direct convolution model. Although the directivity obtained using the modified convolution model contains inaccuracies at 4 kHz at large angles, it can predict sidelobes which are not shown in the direct convolution model, which is resulted from the aperture effect of the audio sound as characterized by $\mathcal{D}_A$ in Eq. (26).

By comparing different columns of Fig. 2, it is found that the exact solution of the directivity becomes narrower at larger aperture sizes. A similar phenomenon is also observed at higher audio frequencies by comparing different rows of Fig. 2. This is attributed to the aperture factor of both the ultrasound and audio sound, which is determined by k_{ia} $(i = 1, 2)$ and $k_a a$, respectively. It is noted that Westervelt directivity is independent of aperture size as

https://doi.org/10.1121/10.0017361

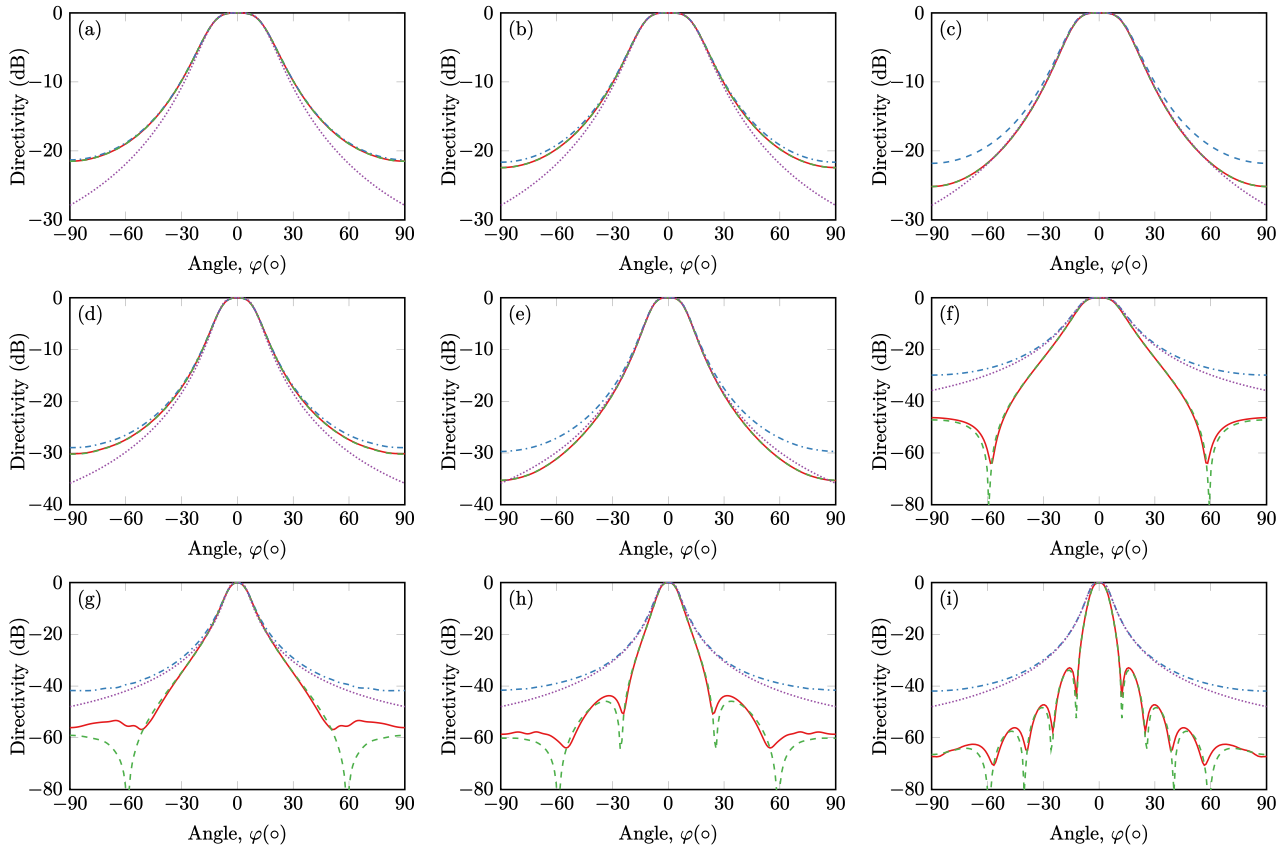

FIG. 2. (Color online) Far field directivity of audio sound generated by a linear PAL with a piston source in a 2D model. Left column, $a = 5$ cm; middle column, $a = 10$ cm; right column, $a = 20$ cm; top row, $f_a = 400$ Hz; middle row, $f_a = 1$ kHz; bottom row, $f_a = 4$ kHz; solid line, exact solution; dashed line, modified convolution model; dashed-dotted line, direct convolution model; dotted line, Westervelt directivity.

shown by Eq. (23) resulting in identical curves at different aperture sizes. The aperture factor of ultrasound is included in the direct convolution model by taking into account ultrasound directivities, so the predictions are more accurate than Westervelt directivity. However, the aperture factor of audio sound is incorrectly captured in the direct convolution model resulting in a deteriorated prediction accuracy as the audio frequency and the aperture size increase. At higher audio frequencies and/or larger aperture sizes, the audio sound can be seen as the radiation from a virtual source in the near field with a transverse dimension of $2a$. This can be approximated by the effective directivity used in the modified convolution model as shown by Eq. (26), so that it outperforms the direct convolution model.

2. Apodized source

The apodized source refers to that the velocity profile of the source is shaded by a weight function. There are various kinds of apodization schemes (see Sec. 3.3 in Ref. [30]). In this work, the cosine window is adopted here,[33] i.e., $u_i(\boldsymbol{\rho}_s) = \cos[\pi y_s/(2a)]$, where $\rho_s \le a$, which represents a vibration mode of a membrane with fixed edges. The far field directivity of ultrasound is then $\mathcal{D}_i(\varphi) = \mathrm{sinc}(k_i a \sin\varphi + \pi/2) + \mathrm{sinc}(k_i a \sin\varphi - \pi/2)$ [see Eq. (3.71) in Ref. 30]. The aperture factor of audio sound is determined by an audio source with a same aperture size and a velocity profile of $u_a(\boldsymbol{\rho}_s) = \cos^2[\pi y_s/(2a)]$. The effective directivity is then $\mathcal{D}_A(\varphi) = 2\mathrm{sinc}(k_a a \sin\varphi) + \mathrm{sinc}(k_a a \sin\varphi + \pi) + \mathrm{sinc}(k_a a \sin\varphi - \pi)$.

Figure 3 shows the audio sound directivities generated by a PAL apodized by a cosine window using different methods. Westervelt directivity is defined only for a piston source, so it is not presented here. It is observed that the direct convolution model is accurate in the vicinity of the mainlobe at 0°, while its accuracy deteriorates at large azimuthal angles. The error of the direct convolution model becomes larger at higher audio frequencies and/or larger aperture sizes because the aperture factor of audio sound is more significant. For example, the 0.1 dB error beam width of the direct convolution model is 34° at 1 Hz when the aperture size is 5 cm, while it decreases to only 6° at 4 kHz when the aperture size is 10 cm. It is interesting to note that the error of the modified convolution model is less than 0.1 dB at all angles at different audio frequencies and aperture sizes, indicating that the 0.1 dB error beam width is 180°. It means that the directivity obtained using the modified convolution model is accurate in all directions for a source apodized by a cosine window, while inaccurate results are obtained at large azimuthal angles for a piston source as shown in Fig. 2. The reason is that the velocity profile of a piston source changes abruptly at the edge $\rho_s = a$ while it is smooth for a source apodized by a cosine window.

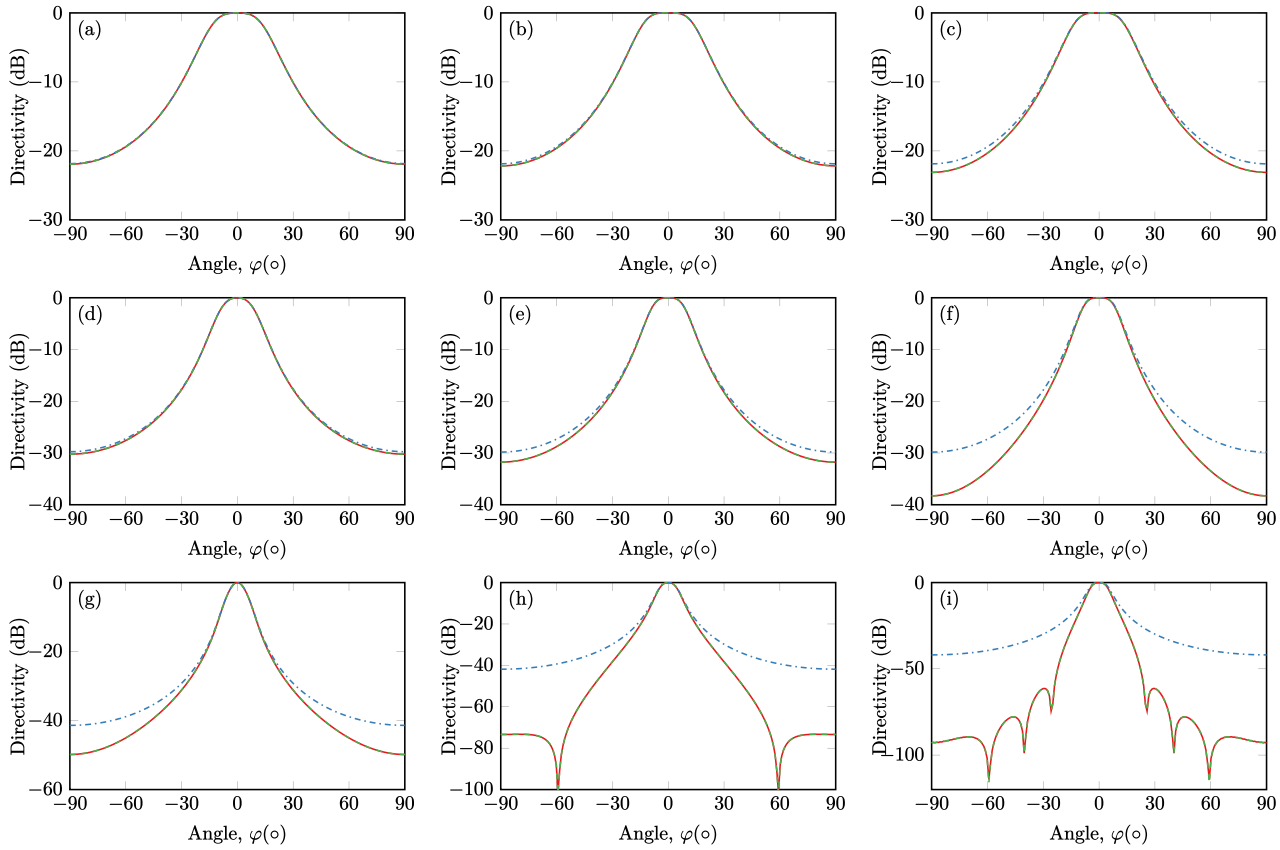

FIG. 3. (Color online) Far field directivity of audio sound generated by a linear PAL apodized by a cosine window. Left column, $a = 5$ cm; middle column, $a = 10$ cm; right column, $a = 20$ cm; top row, $f_a = 400$ Hz; middle row, $f_a = 1$ kHz; bottom row, $f_a = 4$ kHz; solid line, exact solution; dashed line, modified convolution model; dashed-dotted line, direct convolution model.

Accordingly, the ultrasound field generated by a piston source is more complicated and many local maxima and minima appear as shown in Fig. 4, where the normalized axial sound pressure level (SPL) is presented for two kinds of profiles. The complex nonlinear interactions of ultrasound in the near field cannot be well captured by the convolution model for a piston source.

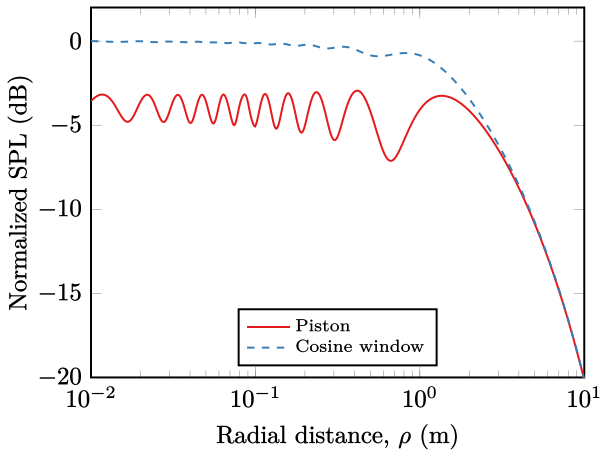

FIG. 4. (Color online) Normalized axial ($\varphi = 90°$) SPL generated by a 2D line source with a half width of $a = 10$ cm at 40 kHz.

3. Steerable source

A 2D steerable PAL is widely investigated in the literature, which aims to steer the highly directional audio beam into a desired direction without the need to mechanically rotate the source.[25] In this work, the velocity profile of ultrasound is assumed to be $u_i(\boldsymbol{\rho}_s) = \exp[i\Re(k_i)y_s \sin\varphi_0]$, where $\Re(\cdot)$ takes the real part of the argument and φ_0 is the steering angle. The far field directivity of ultrasound is then $\mathcal{D}_i(\varphi) = \mathrm{sinc}[\Re(k_i)a(\sin\varphi - \sin\varphi_0)]$. The aperture factor of audio sound is determined by an audio source with a same aperture size and a velocity profile of $u_a(\boldsymbol{\rho}_s) = \exp(ik_a y_s \sin\varphi_0)$. The effective directivity is then $\mathcal{D}_A(\varphi) = \mathrm{sinc}(k_a a(\sin\varphi - \sin\varphi_0))$. Figure 5 shows the directivity obtained using different methods when the steering angle is 15°. It is also observed that the modified convolution model outperforms the direct one especially at high audio frequencies and large aperture sizes. For example, the 1 dB error beam width of the direct convolution model is 29°, 15°, and 7° at 4 kHz when the aperture size is 5, 10, and 20 cm, while it increases 83°, 42°, and 24° for the modified convolution model, respectively. Although the results obtained using the modified convolution model differ from the exact solution at large angles, it can obtain accurate results within the mainlobe and predict the appearance of sidelobes which are resulted from the aperture factor of audio sound.

https://doi.org/10.1121/10.0017361

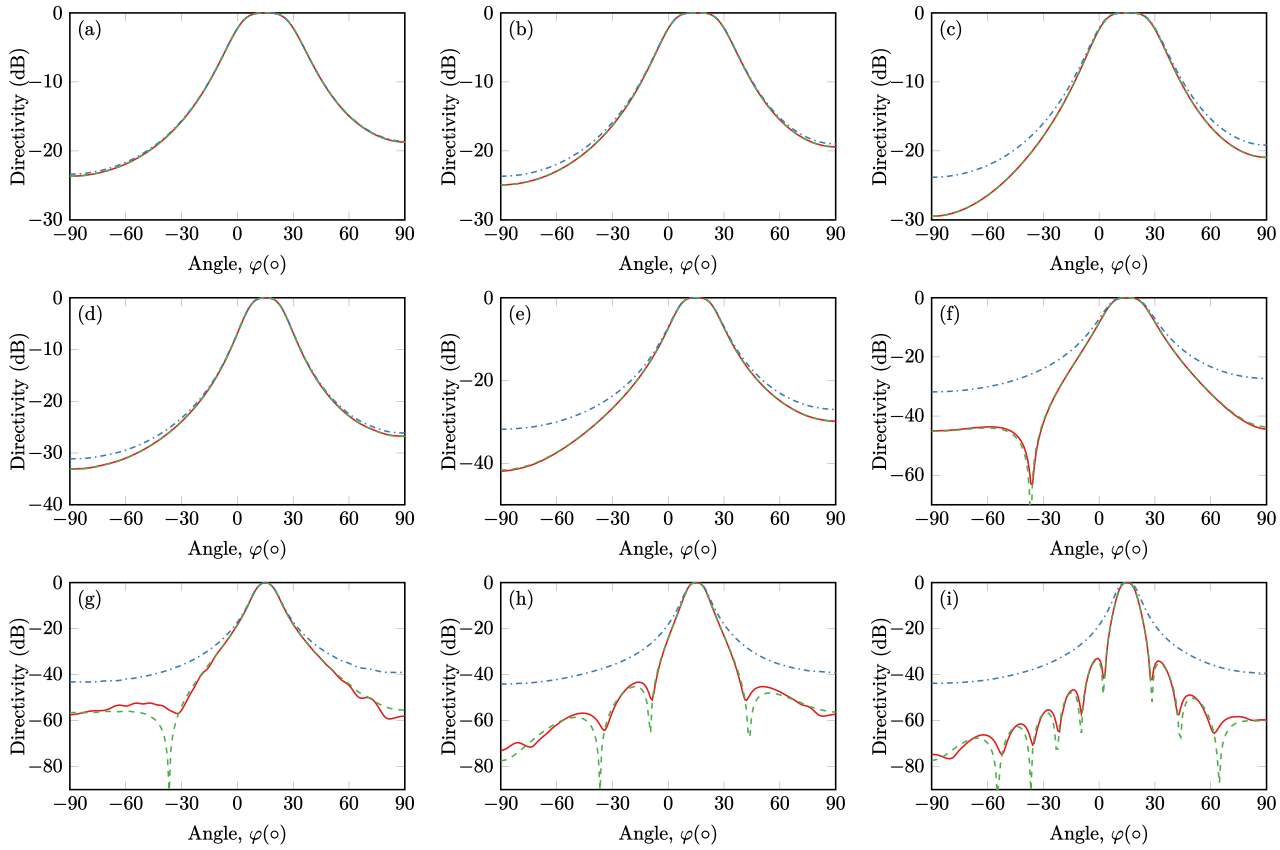

FIG. 5. (Color online) Far field directivity of audio sound generated by a steerable PAL with a steering angle of 15°. Left column, $a = 5$ cm; middle column, $a = 10$ cm; right column, $a = 20$ cm; top row, $f_a = 400$ Hz; middle row, $f_a = 1$ kHz; bottom row, $f_a = 4$ kHz; solid line, exact solution; dashed line, modified convolution model; dashed-dotted line, direct convolution model.

B. 3D model

1. Piston source

For a piston source in a 3D model, the velocity profile is uniform for ultrasound as $u_i(\mathbf{r}_s) = 1$, where $r_s \le a$. Accordingly, the far field directivity of ultrasound is $\mathcal{D}_i(\theta) = \text{jinc}(k_i a \sin\theta)$, where the jinc function $\text{jinc}(x) \equiv 2J_1(x)/x$ and $J_1(x)$ is the Bessel function of order 1. The aperture factor of audio sound is determined by an audio source with a same aperture size and a velocity profile of $u_a(\mathbf{r}_s) = 1$. The effective directivity is then $\mathcal{D}_A(\theta) = \text{jinc}(k_a a \sin\theta)$. Figure 6 shows the audio sound directivities in the plane xOz using different methods. It is noted that the azimuthal angle φ can be either 0° or 180° in the plane xOz, so the directivity as a function of $\theta\cos\varphi$ is presented in the following figures. Although the directivity differs from that generated by a 2D piston source as shown in Fig. 2, similar results are observed that the modified convolution model outperforms Westervelt directivity and the direct convolution model at all cases. For example, the 1 dB error beam width is 110° for the modified convolution model at 4 kHz when the radius is 5 cm, while it is only 16° and 34° for Westervelt directivity and the direct convolution model, respectively. The improvement of the modified convolution model is more significant at high audio frequencies and aperture sizes. At 4 kHz, when the radius is either 10 or 20 cm, the sidelobes can be predicted by the modified convolution model with an acceptable accuracy while they are not predicted by other methods.

2. Apodized source

Here, we consider the quadratic profile for the velocity distribution, i.e., $u_i(\mathbf{r}_s) = [1 - (r_s/a)^2]^{m_i}$, where $r_s \le a$ and the order $m_i = 0, 1, 2, \ldots$. The degenerated quadratic profile with an order of $m_i = 0$ represents a piston source. Higher order quadratic profiles are more realistic in applications.[34,35] For example, the profiles of order $m_i = 1$ and 2 correspond to a simply supported source and a clamped source, respectively.[13] Accordingly, the far field directivity of ultrasound with a quadratic profile of order m_i is $\mathcal{D}_i(\theta) = J_{m_i+1}(k_i a \sin\theta)/(k_i a \sin\theta)^{m_i+1}$.[35] The aperture factor of audio sound is determined by an audio source with a same aperture size and a velocity profile of $u_a(\mathbf{r}_s) = u_1^*(\mathbf{r}_s)u_2(\mathbf{r}_s) = [1 - (r_s/a)^2]^{m_1+m_2}$. The effective directivity is then $\mathcal{D}_A(\theta) = J_{m_1+m_2+1}(k_a a \sin\theta)/(k_a a \sin\theta)^{m_1+m_2+1}$.

Figure 7 shows the audio sound directivities generated by a circular PAL with a quadratic profile of order $m_1 = m_2 = 1$ obtained using different methods. It is observed that the directivity obtained using the direct convolution model differs from the exact solution at angles away from the mainlobe at 0°. The 0.1 dB error beam width of the direct convolution model in Figs. 7(a)–7(i) is 180°, 70°, 34°, 54°,

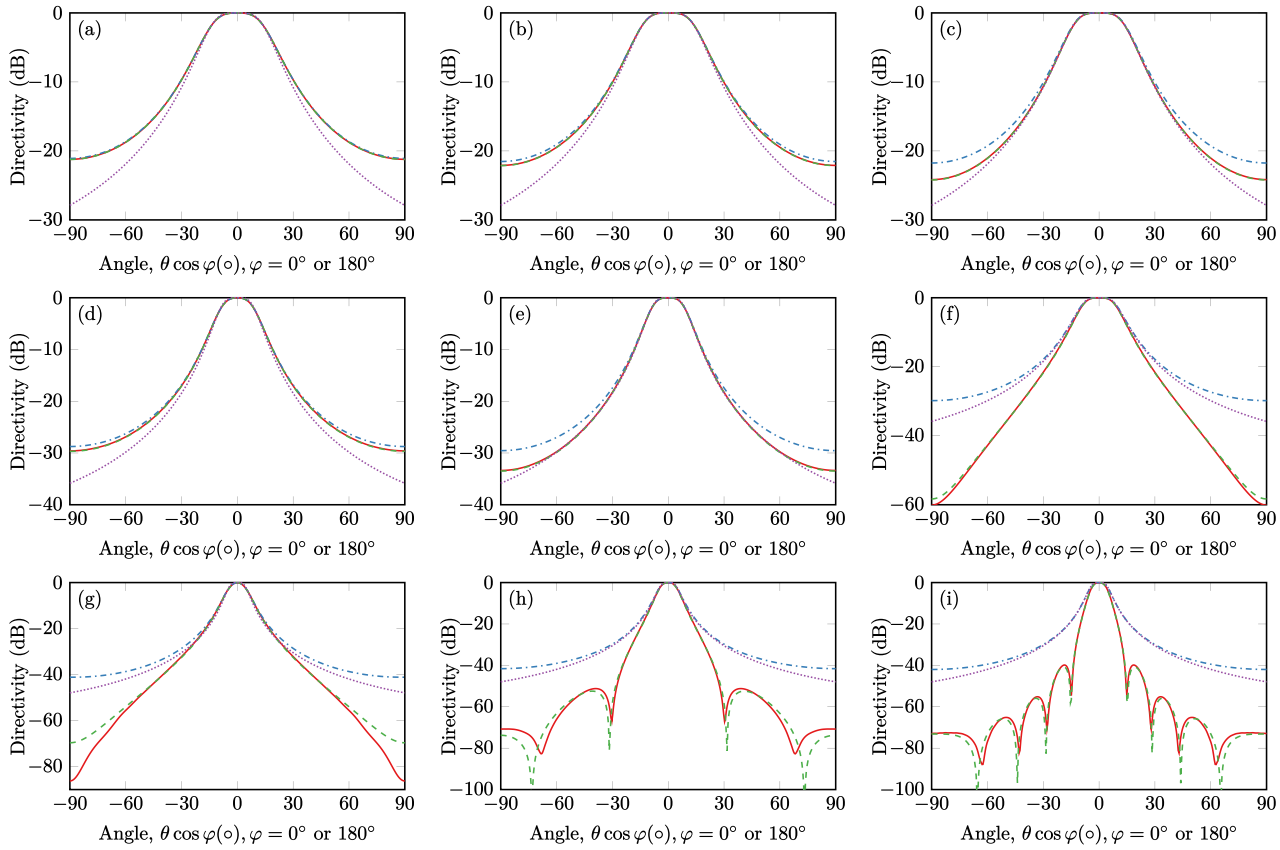

FIG. 6. (Color online) Far field directivity of audio sound generated by a circular PAL with a piston source in a 3D model. Left column, $a = 5$ cm; middle column, $a = 10$ cm; right column, $a = 20$ cm; top row, $f_a = 400$ Hz; middle row, $f_a = 1$ kHz; bottom row, $f_a = 4$ kHz; solid line, exact solution; dashed line, modified convolution model; dashed-dotted line, direct convolution model; dotted line, Westervelt directivity.

26°, 13°, 14°, 7°, and 3°, respectively. The directivity of the modified convolution model agrees well with the exact solution with a 0.1 dB error beam width of 180° in all cases. Similar to the apodized source in the 2D model as shown by Fig. 3, the improvement of the modified convolution model is attributed to the smooth profile at the edge. Figure 8 shows the normalized axial SPL generated by a circular source with a uniform profile (piston) and a quadratic profile of order 1 at 40 kHz. It can be found the ultrasound field with a piston source fluctuates more significantly in the near field, so that the nonlinear interactions in the near field are more difficult to be captured in the convolution model.

3. Steerable source

A 3D steerable PAL means that the directional audio beam can be steered in both azimuthal φ and zenithal θ directions, which is more flexible than a 2D steerable PAL as introduced in Sec. IV A 3. For a steerable source in a 3D model, the steering direction is assumed to be determined by a unit vector of $\hat{\mathbf{s}} = (\cos\varphi_0 \sin\theta_0, \sin\varphi_0 \sin\theta_0, \cos\theta_0)$, where θ_0 and φ_0 are the steering zenithal and azimuthal angles, respectively. The velocity profile is $u_i(\mathbf{r}_s) = \exp[\mathrm{i}\Re(k_i)\mathbf{r}_s \cdot \hat{\mathbf{s}}] = \exp[\mathrm{i}\Re(k_i)(x_s \cos\varphi_0 \sin\theta_0 + y_s \sin\varphi_0 \sin\theta_0)]$. The directivity of ultrasound is then obtained as $\mathcal{D}_i(\theta,\varphi) = \mathrm{jinc}(\Re(k_i)a\Phi(\theta,\varphi))$, where $\Phi(\theta,\varphi) \equiv \sqrt{(\cos\varphi\sin\theta - \cos\varphi_0\sin\theta_0)^2 + (\sin\varphi\sin\theta - \sin\varphi_0\sin\theta_0)^2}$. The aperture factor of audio sound is determined by an audio source with a same aperture size and a velocity profile of $u_a(\mathbf{r}_s) = \exp(\mathrm{i}k_a\mathbf{r}_s \cdot \hat{\mathbf{s}})$. The effective directivity is then $\mathcal{D}_A(\theta,\varphi) = \mathrm{jinc}(k_a a\Phi(\theta,\varphi))$.

Figure 9 shows the directivity in the plane xOz obtained using different methods for a 3D steerable PAL. Because the exact solution is quite challenging at large aperture sizes for a PAL with a nonaxisymmetric profile,[29] the zenithal steering angle θ_0 is set as 10°, 5°, and 2.5°, for $a = 5$ cm, $a = 10$ cm, $a = 20$ cm, respectively. At a low frequency of 400 Hz, the 0.1 dB error beam width of the modified convolution model is 180°, while that of the direct convolution model is 135°, 52°, and 25° when the aperture size is 5, 10, and 20 cm, respectively. At a high frequency of 4 kHz, the 1 dB error beam width of the direct convolution model is only 35°, 10°, and 7°, while that of the modified convolution model is 130°, 50°, and 25°, when the aperture size is 5, 10, and 20 cm, respectively. It is also observed that the modified convolution model still outperform the direct convolution model for a 3D steerable PAL especially at high audio frequencies and large aperture sizes.

C. Computational efficiency

In this subsection, the computational efficiency of proposed methods is compared based on the numerical results

https://doi.org/10.1121/10.0017361

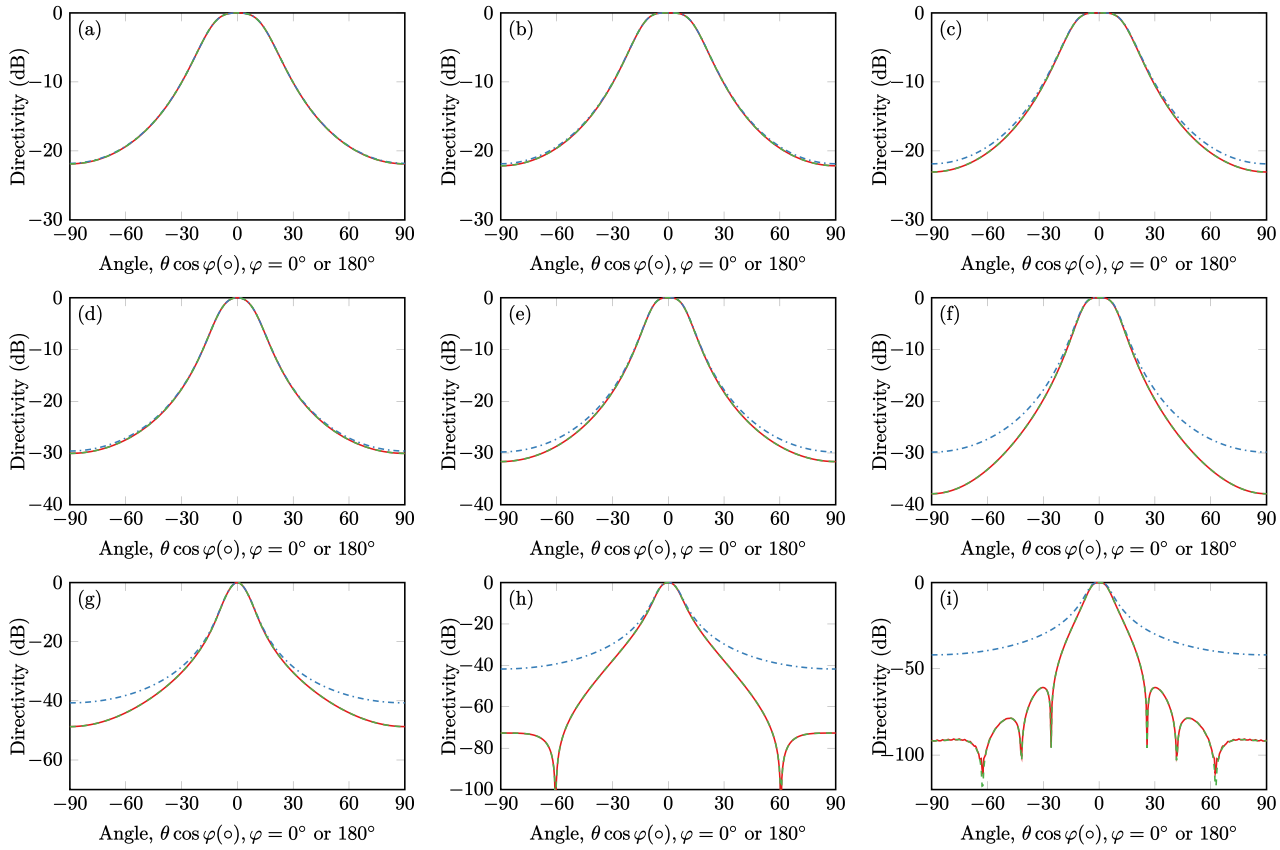

FIG. 7. (Color online) Far field directivity of audio sound generated by a circular PAL with a quadratic profile of order $m_1 = m_2 = 1$ in a 3D model. Left column, $a = 5$ cm; middle column, $a = 10$ cm; right column, $a = 20$ cm; top row, $f_a = 400$ Hz; middle row, $f_a = 1$ kHz; bottom row, $f_a = 4$ kHz; solid line, exact solution; dashed line, modified convolution model; dashed-dotted line, direct convolution model.

obtained using a personal computer with an AMD Ryzen™ Threadripper™ 3960X (Santa Clara, CA) central processing unit (CPU) and 256 GB of random access memory (RAM). The calculation time of the exact solution and the convolution models is compared in Table I for six configurations presented in this section. In all configurations, the elapsed calculation time is the calculation of the directivity at 100 field points. For simplicity, only the case when the audio frequency $f_a = 4$ kHz and the aperture size $a = 20$ cm is presented, which is the most time consuming because of the large $k_a a$. The corresponding results are plotted in Figs. 2(i), 3(i), 5(i)–7(i), and 9(i). It is noted that both direct and modified convolution models have the same computational complexity, so the last column in Table I represents the calculation time for both of them. It can be observed in Table I that the convolution models are at least more than 150 times faster than the exact solution for 2D and 3D axisymmetric configurations. For a 3D steerable source which has a nonaxisymmetric profile, the calculation time of the convolution models is only 0.12 s, while it is even more than to obtain a converged result for the exact solution. It is concluded that the proposed modified convolution model provides a computationally efficient prediction method with an acceptable accuracy for calculating the far field directivity of a PAL.

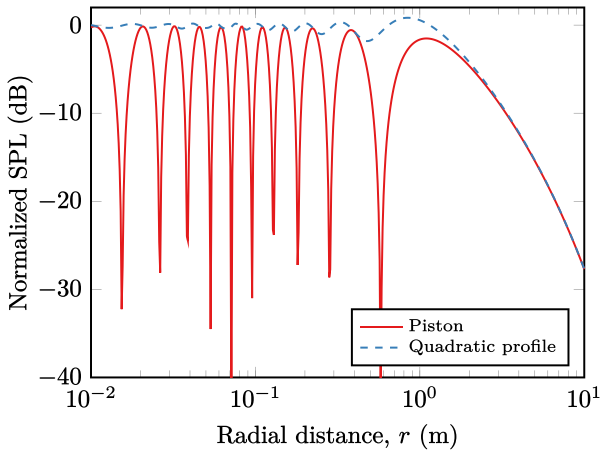

FIG. 8. (Color online) Normalized axial ($\theta = 0°$) SPL generated by a circular source with a radius of $a = 10$ cm at 40 kHz.

V. CONCLUSION

This work derived 2D, 3D, and 3D axisymmetric convolution models for calculating the far field directivity based on the quasilinear solution of Westervelt equation. The key is to approximate the complicated ultrasound pressure in the near field by its inward-extrapolated far field pressure. The direct convolution model is expressed as linear and spherical

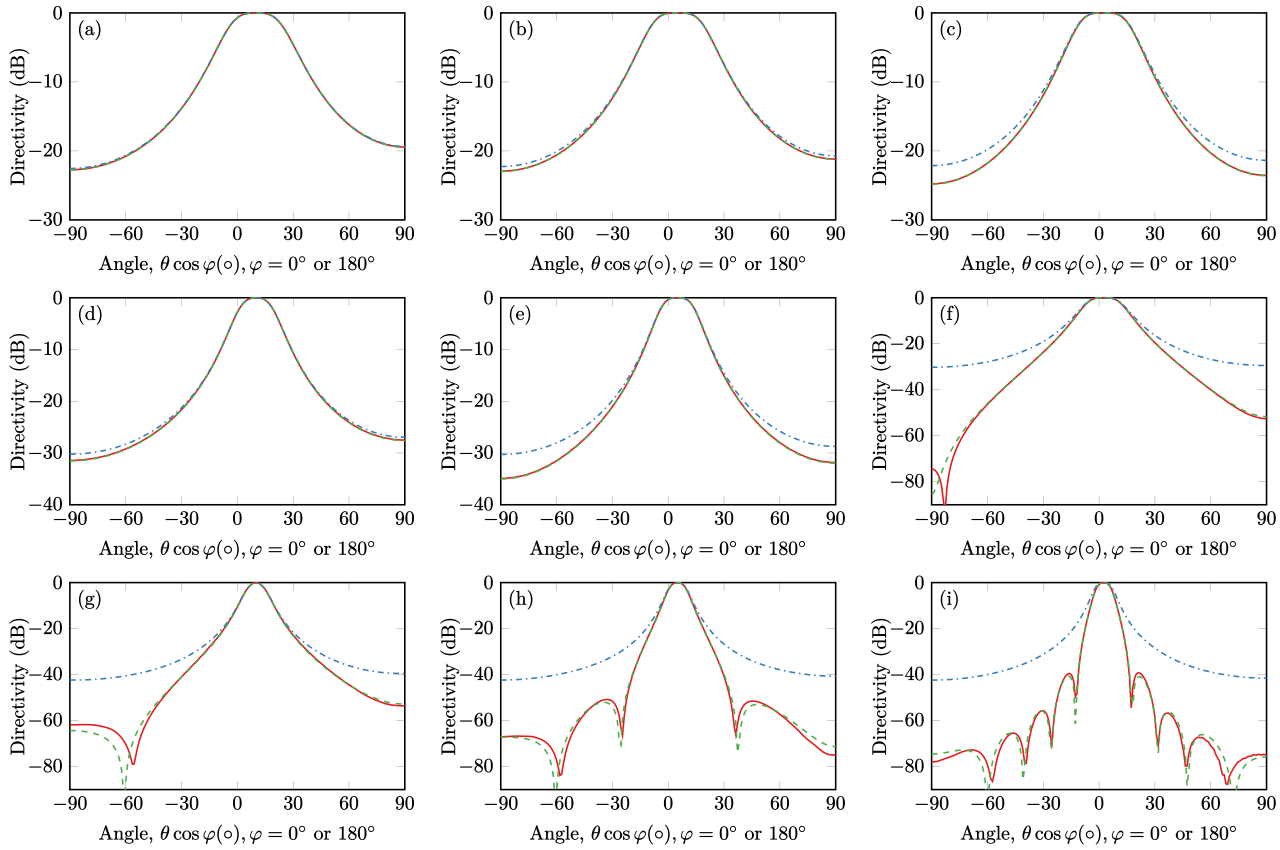

FIG. 9. (Color online) Far field directivity of audio sound generated by a circular steerable PAL with azimuthal and zenithal steering angles of (θ_0, φ_0). Left column, $a = 5$ cm and $(\theta_0, \varphi_0) = (10°, 0°)$; middle column, $a = 10$ cm and $(\theta_0, \varphi_0) = (5°, 0°)$; right column, $a = 20$ cm and $(\theta_0, \varphi_0) = (2.5°, 0°)$; top row, $f_a = 400$ Hz; middle row, $f_a = 1$ kHz; bottom row, $f_a = 4$ kHz; solid line, exact solution; dashed line, modified convolution model; dashed-dotted line, direct convolution model.

convolution of the ultrasound directivity and Westervelt directivity for 2D and 3D models, respectively. A modified convolution model was proposed by multiplying the directivity obtained using the direct convolution model with an effective directivity resulted from the aperture factor of audio sound. The effective directivity is obtained by an audio source with a same aperture size and a velocity profile of the product of that of ultrasonic sources at two frequencies. Accordingly, both convolution models are much more computationally efficient than the exact solution of evaluating the quasilinear solution of Westervelt equation. It is observed that the directivity obtained using the direct convolution model differs from the exact solution at angles away from the mainlobe, but it can be addressed by the modified convolution model. The 2D direct convolution model has been widely used in analyzing the far field directivity of a linear phased array PAL for steering the audio beams.[7,25] The proposed modified convolution model in this work provides a more accurate tool for this kind of problem. Moreover, it can be used for the analysis of a 3D steerable PAL which can steer the directional audio beam in both azimuthal and zenithal directions and has not been investigated in the existing literature.

TABLE I. Comparison of the calculation time of the exact solution and the proposed convolution models. In all configurations, the directivity at 100 field points is calculated, where the audio frequency $f_a = 4$ kHz and the aperture size $a = 20$ cm.

Configuration	Plotted in	Convolution models (s)	Exact solution
2D piston source	Fig. 2(i)	0.13	23.42 s
2D apodized source	Fig. 3(i)	0.06	22.02 s
2D steerable source	Fig. 5(i)	0.16	25.21 s
3D piston source	Fig. 6(i)	0.11	31.58 s
3D apodized source	Fig. 7(i)	0.21	32.17 s
3D steerable source	Fig. 9(i)	0.12	>1 day

ACKNOWLEDGMENTS

H. Z. and J. L. gratefully acknowledge the financial support from the National Natural Science Foundation of China (Grant No. 12274221). D. Z. gratefully acknowledges the financial support from the National Natural Science Foundation of China (Grant No. 11934009).

APPENDIX: EVALUATION OF THE INTEGRAL GIVEN BY EQ. (36)

For simplicity, the integral given by Eq. (36) is defined as I, which can be rewritten as

https://doi.org/10.1121/10.0017361

$$I = \frac{1}{2\pi\left[1 - \mathrm{i}k_\mathrm{a}\alpha_\mathrm{t}^{-1}(1 - \cos\theta\cos\theta_\mathrm{v})\right]}\int_0^{2\pi}\frac{\mathrm{d}\varphi_\mathrm{v}}{1 + A\cos\varphi_\mathrm{v}}, \quad \text{(A1)}$$

where

$$A = \frac{\mathrm{i}k_\mathrm{a}\alpha_\mathrm{t}^{-1}\sin\theta\sin\theta_\mathrm{v}}{1 - \mathrm{i}k_\mathrm{a}\alpha_\mathrm{t}^{-1}(1 - \cos\theta\cos\theta_\mathrm{v})}. \quad \text{(A2)}$$

It is easy to show that $|A| < 1$. By using the result of example 11.3.6 in Ref. 36, the integral given by the form in Eq. (A1) can be evaluated using the residue theorem to give

$$I = \frac{1}{1 - \mathrm{i}k_\mathrm{a}\alpha_\mathrm{t}^{-1}(1 - \cos\theta\cos\theta_\mathrm{v})}\frac{1}{\sqrt{1 - A^2}}. \quad \text{(A3)}$$

After substituting Eq. (A2) into Eq. (A3) and rearranging the result, the integral can be simplified to the right-hand side of Eq. (36).

[1]W.-S. Gan, J. Yang, and T. Kamakura, "A review of parametric acoustic array in air," Appl. Acoust. **73**(12), 1211–1219 (2012).
[2]K. G. Foote, "Reflections on 'Parametric acoustic array,' source of virtual-array sonars," J. Acoust. Soc. Am. **150**(1), R1–R2 (2021).
[3]N. Tanaka and M. Tanaka, "Active noise control using a steerable parametric array loudspeaker," J. Acoust. Soc. Am. **127**(6), 3526–3537 (2010).
[4]J. Zhong, T. Zhuang, R. Kirby, M. Karimi, H. Zou, and X. Qiu, "Quiet zone generation in an acoustic free field using multiple parametric array loudspeakers," J. Acoust. Soc. Am. **151**(2), 1235–1245 (2022).
[5]Y. Ogami, M. Nakayama, and T. Nishiura, "Virtual sound source construction based on radiation direction control using multiple parametric array loudspeakers," J. Acoust. Soc. Am. **146**(2), 1314–1325 (2019).
[6]B. Castagnède, A. Moussatov, D. Lafarge, and M. Saeid, "Low frequency *in situ* metrology of absorption and dispersion of sound absorbing porous materials based on high power ultrasonic non-linearly demodulated waves," Appl. Acoust. **69**(7), 634–648 (2008).
[7]C. Shi, Y. Kajikawa, and W.-S. Gan, "Generating dual beams from a single steerable parametric loudspeaker," Appl. Acoust. **99**, 43–50 (2015).
[8]N. Hahn, J. Ahrens, and C. Andersson, "Parametric array using amplitude modulated pulse trains: Experimental evaluation of beamforming and single sideband modulation," in *Audio Engineering Society Convention 151* (Audio Engineering Society, 2021), pp. 1–7.
[9]A. Okano and Y. Kajikawa, "Phase control of parametric array loudspeaker by optimizing sideband weights," in *ICASSP 2022 - 2022 IEEE International Conference on Acoustics, Speech and Signal Processing (ICASSP)* (2022), pp. 31–35.
[10]H. Wang, J. Tang, Z. Wu, and Y. Liu, "A multi-beam steerable parametric array loudspeaker for distinct audio content directing," IEEE Sens. J. **22**(13), 13640–13647 (2022).
[11]J. Zhong, R. Kirby, and X. Qiu, "The near field, Westervelt far field, and inverse-law far field of the audio sound generated by parametric array loudspeakers," J. Acoust. Soc. Am. **149**(3), 1524–1535 (2021).
[12]S. I. Aanonsen, T. Barkve, J. N. Tjøtta, and S. Tjøtta, "Distortion and harmonic generation in the nearfield of a finite amplitude sound beam," J. Acoust. Soc. Am. **75**(3), 749–768 (1984).
[13]M. Červenka and M. Bednařík, "A versatile computational approach for the numerical modelling of parametric acoustic array," J. Acoust. Soc. Am. **146**(4), 2163–2169 (2019).
[14]M. Červenka and M. Bednařík, "An algebraic correction for the Westervelt equation to account for the local nonlinear effects in parametric acoustic array," J. Acoust. Soc. Am. **151**(6), 4046–4052 (2022).
[15]J. Zhong, R. Kirby, and X. Qiu, "A spherical expansion for audio sounds generated by a circular parametric array loudspeaker," J. Acoust. Soc. Am. **147**(5), 3502–3510 (2020).
[16]J. Zhong, R. Kirby, M. Karimi, and H. Zou, "A cylindrical expansion of the audio sound for a steerable parametric array loudspeaker," J. Acoust. Soc. Am. **150**(5), 3797–3806 (2021).
[17]J. Yang, K. Sha, W.-S. Gan, and J. Tian, "Modeling of finite-amplitude sound beams: Second order fields generated by a parametric loudspeaker," IEEE Trans. Ultrason., Ferroelect., Freq. Contr. **52**(4), 610–618 (2005).
[18]M. Červenka and M. Bednařík, "Non-paraxial model for a parametric acoustic array," J. Acoust. Soc. Am. **134**(2), 933–938 (2013).
[19]P. J. Westervelt, "Parametric acoustic array," J. Acoust. Soc. Am. **35**(4), 535–537 (1963).
[20]H. O. Berktay, "Possible exploitation of non-linear acoustics in underwater transmitting applications," J. Sound Vib. **2**(4), 435–461 (1965).
[21]H. O. Berktay and D. J. Leahy, "Farfield performance of parametric transmitters," J. Acoust. Soc. Am. **55**(3), 539–546 (1974).
[22]W.-S. Gan, J. Yang, K.-S. Tan, and M.-H. Er, "A digital beamsteerer for difference frequency in a parametric array," IEEE/ACM Trans. Audio, Speech, Lang. Process. **14**(3), 1018–1025 (2006).
[23]C. Shi and W.-S. Gan, "Product directivity models for parametric loudspeakers," J. Acoust. Soc. Am. **131**(3), 1938–1945 (2012).
[24]M. F. Hamilton, J. N. Tjøtta, and S. Tjøtta, "Nonlinear effects in the farfield of a directive sound source," J. Acoust. Soc. Am. **78**(1), 202–216 (1985).
[25]C. Shi and Y. Kajikawa, "A convolution model for computing the far-field directivity of a parametric loudspeaker array," J. Acoust. Soc. Am. **137**(2), 777–784 (2015).
[26]C. Shi, Y. Wang, H. Xiao, and H. Li, "Extended convolution model for computing the far-field directivity of an amplitude-modulated parametric loudspeaker," J. Phys. D: Appl. Phys. **55**(24), 244002 (2022).
[27]O. Guasch and P. Sánchez-Martín, "Far-field directivity of parametric loudspeaker arrays set on curved surfaces," Appl. Math. Model. **60**, 721–738 (2018).
[28]K. G. Foote, "Discriminating between the nearfield and the farfield of acoustic transducers," J. Acoust. Soc. Am. **136**(4), 1511–1517 (2014).
[29]J. Zhong, R. Kirby, M. Karimi, and H. Zou, "A spherical wave expansion for a steerable parametric array loudspeaker using Zernike polynomials," J. Acoust. Soc. Am. **152**(4), 2296–2308.
[30]L. W. Schmerr, Jr., *Fundamentals of Ultrasonic Phased Arrays* (Springer, New York, 2014).
[31]P. J. Roddy and J. D. McEwen, "Sifting convolution on the sphere," IEEE Signal Process. Lett. **28**, 304–308 (2021).
[32]ISO 9613-1:1993, "Acoustics — Attenuation of sound during propagation outdoors — Part 1: Calculation of the absorption of sound by the atmosphere" (International Organization for Standardization, Geneva, 1993).
[33]J. Assaad and J. M. Rouvaen, "Numerical evaluation of the far-field directivity pattern using the fast Fourier transform," J. Acoust. Soc. Am. **104**(1), 72–80 (1998).
[34]M. Greenspan, "Piston radiator: Some extensions of the theory," J. Acoust. Soc. Am. **65**(3), 608–621 (1979).
[35]R. M. Aarts and A. J. E. M. Janssen, "On-axis and far-field sound radiation from resilient flat and dome-shaped radiators," J. Acoust. Soc. Am. **125**(3), 1444–1455 (2009).
[36]S. Hassani, *Mathematical Physics: A Modern Introduction to Its Foundations*, 2nd ed. (Springer International Publishing, Cham, 2013).